PERIODICA POLYTECHNICA SER. TRANSP. ENG. VOL. 34, NO. 1–2, PP. 35–58 (2006)

MODELLING OF GEAR CHANGING BEHAVIOUR

László LOVAS*, Daniel PLAY**, János MÁRIALIGETI* and
Jean-François RIGAL***

*Department of Vehicle Parts and Drives
Budapest University of Technology and Economics
H–1111 Budapest, Bertalan L. u. 2.
Phone: +36/1-463-17-39
e-mail: lovas@kge.bme.hu, marial@kge.bme.hu
**Department of Industrial Engineering, bât. Jules Verne
*** LaMCoS, GMC, bât. Joseph Jacquard
INSA-Lyon
20, av. Albert Einstein, F-69621 Villeurbanne Cedex
Phone: +33/4-72-43-64-78, +33/4-72-43-82-88
e-mail: daniel.play@insa-lyon.fr, jean-francois.rigal@insa-lyon.fr

Received: July 19, 2005

Abstract

This paper deals with the modelling of the gear changing behaviour. After presentation of the main synchronizer tasks, the state of the art is described. Reconsideration of the gear changing process allows better definition of synchronizer working phases. Based on this, a numerical simulation software of the synchronizer behaviour has been realized. Phenomena of angular velocity synchonization and second bump in gear changing force are modelled in details. Various mechanical behaviour influencing phenomena are taken into consideration with large number of input parameters. The software is validated with literature data. Then, it is used to investigate the effect of main parameters considered with gear changing process for a 5 speed manual car gearbox. Effects of gear changing force, synchronized inertia and initial angular velocity difference variations are shown. Visualization of parameter effects such as angle error of synchronizer cone and relative position of gear splines and sleeve splines help for better understanding of gearbox behaviour during gear changing.

Keywords: gearbox, synchronization, numerical simulation, parameter study, second bump.

1. Introduction

Manual car gearbox synchronizers are rather complicated mechanical structures. They assume the connection of three main parts of the mechanical transmission (*Fig. 7*). The synchronized side of the transmission is constituted by the disengaged clutch plate, the input shaft of the gearbox and the connected gears. Synchronizing side is composed of mechanical parts up to the wheels of the car. The manual gear changing mechanism (*Fig. 1*) is generally constituted by forks and fork support axes moved by either actuators or hand.

As the dynamical behaviour of these three mechanical subsystems is rather complicated to simulate because of the large number of elements, for a first approach, the following study concentrates on the synchronizer behaviour. Manual

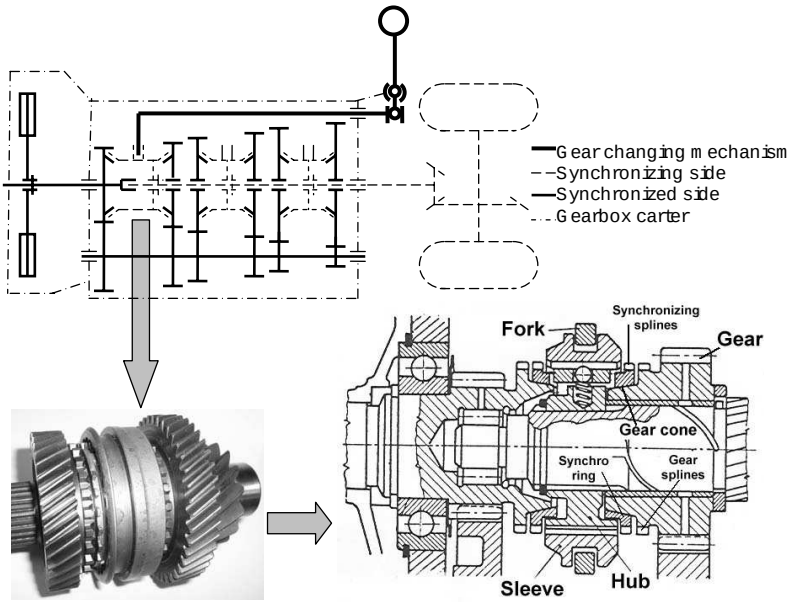

Fig. 1. Structure of the numerical simulation software

gearbox synchronizers have the following tasks:

- Making disappear the angular velocity difference between the synchro hub and the gear to be engaged (*Fig. 1*). This task is called 'synchronization', and it is realized usually by friction, via conical clutches.
- Impeaching the engagement of the gear while the angular velocity difference exists. This task is called 'interdiction'.
- Connecting hub and gear, by gear splines, via sleeve, in order to allow power transmission when the gear changing is realized. For this task, synchronizers must allow the displacement of the synchro sleeve between the synchronizing splines (*Fig. 1*) of the synchro ring to reach gear splines, and between the splines of the gear.

Synchronization of angular velocity is usually obtained by conical friction clutches, while the power transmission is usually realized by spline coupling. Depending on transmitted torque, one, two or three conical surfaces are applied. Obviously, many technical solutions exist but the same nature of problems is found. In this paper, the Borg-Warner type synchronizer with one conical surface clutch will be considered (*Fig. 1*).

At first a short description of the successive phases of synchronizer behaviour is given. Then, numerical simulation software is briefly presented. Finally, numerical simulation results are presented and discussed.

2. State of the Art

Although synchronizers had been used since the late '20s, scientific papers describing their behaviour appeared a couple of decades later. In the late '60s, a global description [15] was given, using simple mechanical equations for describing synchronisation and interdiction, based on large technical experiences. In the early '80s, effect of different linings on clutch conical surfaces was studied [7, 12, 14]. Increase of transmitted power leaded to introduce new developments like multicone synchronizers, again using simple mechanical theory [1, 6, 13, 16]. During the last decade, simulations of global mechanical behaviour were made based on classical softwares (Matlab Simulink, Adams) [2, 4, 5].

New synchronizer evolutions as well as increase of transmitted power and the need for actuating load control give new technical problems to answer. For example, a high gear changing force peak is sometimes experimentally seen after the synchronization phase. This peak is called the second bump. This second bump axial force amplitude can not be clearly explained and thus, is difficult to be simulated. The appearance of the second bump, as well as its size seems to be random phenomena [10]. It is also supposed that this force is responsible for cracking noise during gear changing. Further, some other phenomena are not clearly explained such as wear of coupling splines chamfered ends situated on synchro ring. These not fully understood phenomena make difficult the optimization of synchronizer performances. Consequently all the process and mechanical modelling were reconsidered more in details.

3. Presentation of Working Phases of the Synchronizer

From the point of view of power transmission, synchronizers have two states: either they transmit power or they do not transmit power. Generally one synchronizer makes possible to engage two 'speeds' (ex: 1-2 or 5-6), it has two geometrical position, when the power transmission is possible. For example, either the gear 1 is engaged or the gear 2 is engaged. The third geometrical position is when there is no power transmission. This position is situated between the two engaged positions and is called neutral position. Positions can be set with the axial displacement of the sleeve part (*Fig. 1*). To change from one engaged speed to the another engaged speed with the same synchronizer it is necessary to pass through the neutral position. In this paper, successive phases of gear changing are discussed from the neutral position to the final engagement. This period can be divided into eight phases governed by the sleeve axial displacement (*Fig. 2*):

1. First free fly: starting of the sleeve displacement from the neutral position, gear is not synchronized.
2. Start of the angular velocity synchronization.
3. Angular velocity synchronization.
4. Turning the synchro ring.

5. Second free fly: gear has been already synchronized.
6. Start of the second bump: ending up with an eventual peak force.
7. Turning the gear: second bump.
8. Final free fly: spline coupling is engaged.

Distinction must be made between the so called free fly phases and the other phases. During free fly phases, the sleeve moves forward axially from the previous working position to the next working position without any other function. Doing this, it has to win only friction resistances, and needs small external changing force. In the non free fly positions, sleeve must modify position or angular velocity of transmission parts. For these phases, high external changing force is generally needed.

Detailed analysis of the working phases can be found in [10].

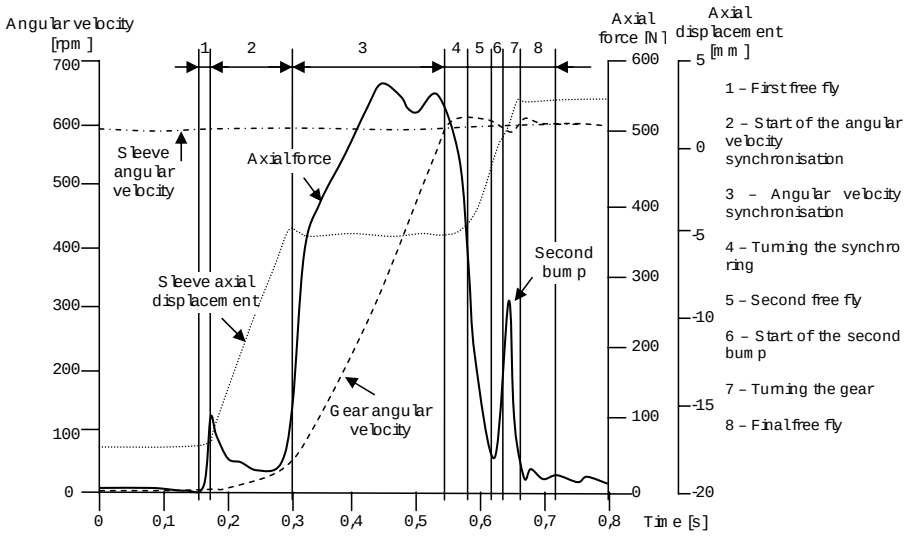

Fig. 2. Definition of working phases during gear changing

Start of the second bump (6) and turning of the gear (7) phases contain the so called 'second bump' or 'double bump' phenomenon. It appears as a sudden axial peak force, shortly after the complete synchronization of the gear to be engaged. Experiences [9] show that size of the peak force varies randomly, hence it is difficult to predict it. This phenomenon is well known in the literature [2, 13].

The period in which the second bump appears is covered by the two aforementioned phases. It is assumed that peak forces can appear in both phases. Given the very short duration of each phase, it is difficult to determine with measures in which phase the force peak appeared. It is also assumed that origins of the second bump can be found at the end of the synchronization phase. One of the origins is that the synchro ring remains stuck on the gear cone at the end of the synchronization. Surface geometry, conicity angle of the surface pairs and the tribological properties

have influence on the intensity of sticking, as described in [8] and [11]. This can be the origin of a peak force at the end of the start of the second bump (6) phase. The relative position of the sleeve splines and the gear splines in the moment of the sticking is the second origin (see *Fig. 11*). This relative position can be the origin of a force peak during the turning of the gear (7) phase. These phenomena are discussed later in this paper.

4. Presentation of the Simulation Software

The numerical simulation model was developed under Delphi environment (Pascal language) through a modular structure. Each module corresponds to one of the previously mentioned working phases. The modular structure allows to study each working phase in a desired level of mechanical behaviour description, and to modify this level depending on local conditions. In each module, iteration loops permit to calculate the variation of parameters describing the behaviour of the parts. Main modules and iteration loops are presented in *Fig. 3*.

The governing parameters are either the axial velocity or the axial force applied on the sleeve. Only one of them is applied for a specific numerical working phase simulation, depending on the studied working phase and the actual position of the parts [11]. The software has more than 60 input parameters that insure high flexibility of use and permit adaptations to various boundary conditions (*Fig. 4*).

The first group of input parameters contains the characteristics of the synchronizer. Large number of geometrical parameters are taken into consideration, followed by dynamical, thermodynamical and tribological parameters. Cone and spline geometry are also detailed. The second group of input parameters contains parameters of the gearbox. Each shaft, gear and bearing is described with kinematical and dynamical parameters. A third group of parameters contains data of the gearbox lubricant. Variations of viscosity are taken into consideration upon gearbox and synchro cone temperature. A fourth group of input data contains description of dynamics of the synchronizing side and of the gear changing mechanism. The last group of parameters contains parameters for describing the stick-slip motion on synchronizer cones and splines. Moreover, effect of gearbox architecture is also taken into consideration, as it defines lubricant quantity and synchronized inertia.

To demonstrate the performance of the simulation software, numerical results were compared to measured data published in the literature [3]. As expected, numerical simulation and measurement data present similar characteristics in many zones, either in the axial force vs. time curve or in the angular velocity vs. time curve. A first zone is the simulation of angular velocity synchronization, where a constant axial force of 240 N is imposed. This value is the mean value of the measured axial force value. The second zone is the second bump zone. Using input parameters issue from measurements on the gear cone and the synchro ring cone, a 700 N second bump of axial force can be calculated (*Fig. 5*). This value is similar to the amplitude of the measured second bump load. Further similarity can be found

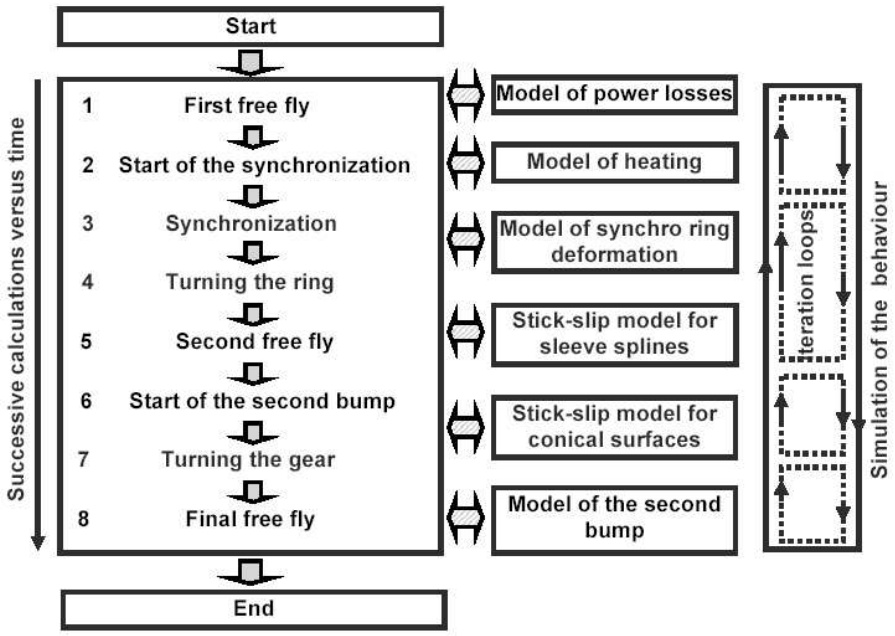

Fig. 3. Structure of the numerical simulation software

in the angular velocity curves.

The measured gear angular velocity presents a desynchonization period after reaching the synchonization point [3] (*Fig. 6*). This desynchonization period is interpreted to correspond to the simulated turning phase of the synchro ring (*Fig. 5*). The measured angular velocity desynchonization is in the order of 10 rpm [3]. Similar value is obtained by numerical simulation (*Fig. 6*). This is a first peak on the simulated and the measured angular velocity curves, after the synchonization point. Then, there is a second desynchonization in the measured angular velocity curve [3]. This desynchonization is assumed to correspond to the simulated turning phase of the gear, where the second bump peak force appears.

5. Study of Some Parameters of Gear Changing

Gear changing process depends on multiple factors. The most important factors are synchronized inertia, initial angular velocity difference and gearbox power losses. They all can be different depending on gearbox architecture. The following simulation data come from an industrial case of a 5 speed JH gearbox (*Fig. 7*).

For a given gearbox, inertia to be synchronized decreases with the increasing speed number: the higher is the inertia of the first gear, the lower is the inertia of

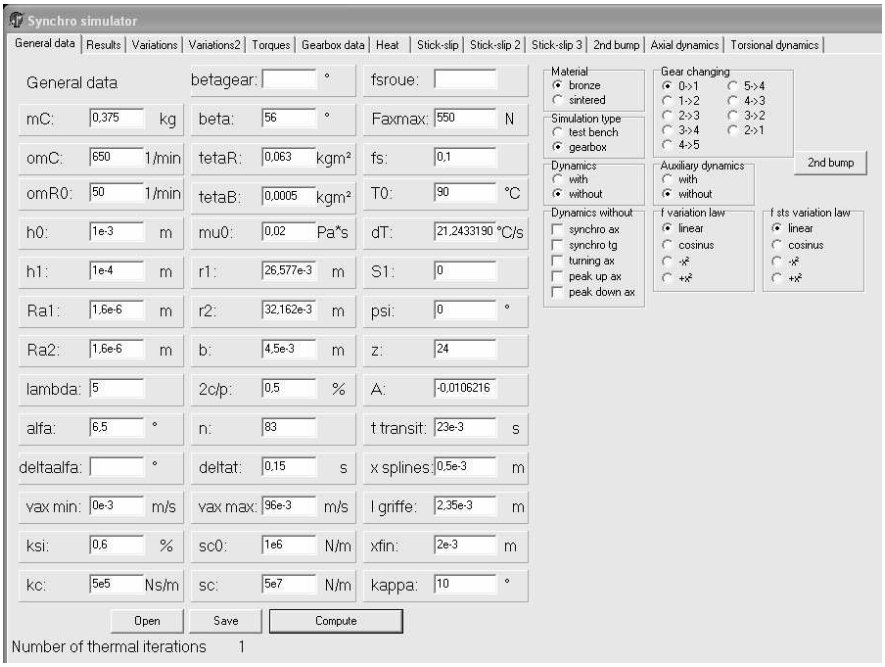

Fig. 4. Software input parameter screen

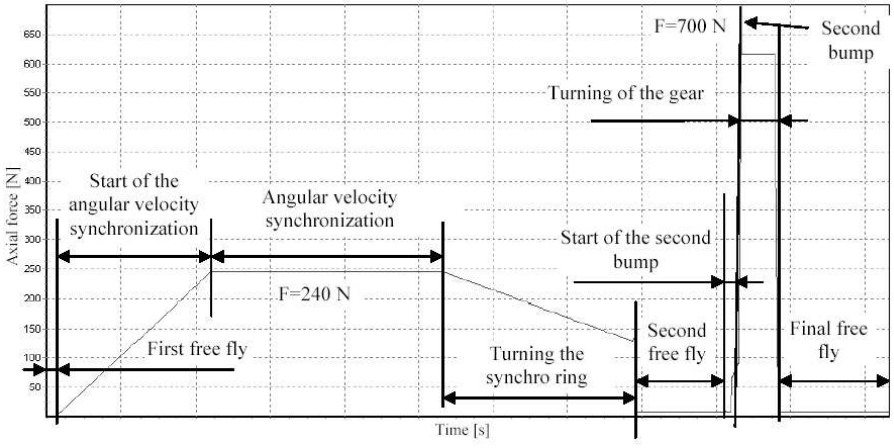

Fig. 5. Axial force vs. time, simulation (input conditions from [3])

the fifth gear. If the initial angular velocity difference in the synchronizer and the changing force are identical, with increasing synchronized inertia, obviously gear

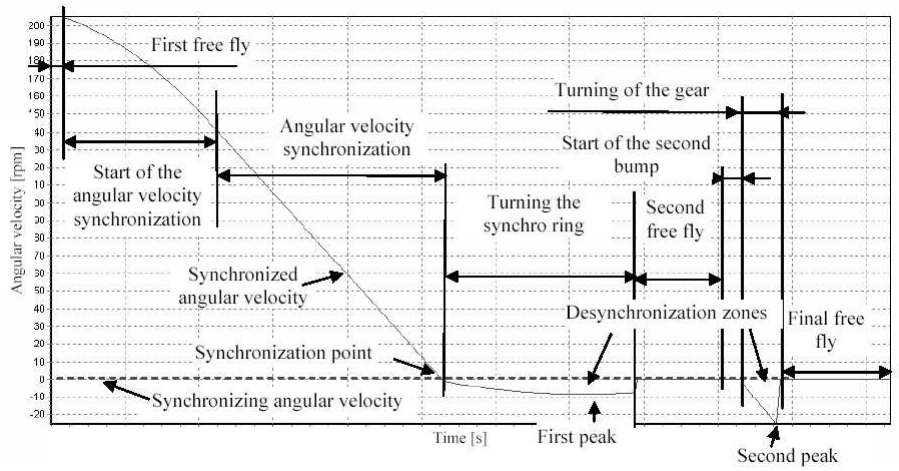

Fig. 6. Gear angular velocity vs. time, simulation (input conditions from [3])

changing time increases (*Table 1*). Similarly, gear changing time increases with increasing angular velocity difference before synchonization (*Fig. 8*). Here, gear changing time is the duration of all the studied phases from the first free fly (1) to the final free fly (8), and it includes synchonization time.

Gear changing conditions vary depending on speeds to be engaged (*Table 1*, *Table 2*). Assuming the same synchronizing force, changing time is proportional with the synchronized inertia. Note that for the same inertia, changing times are different for upshift and downshift. This is attributed to the gearbox power losses. During upshift, synchronized gear slows down. Power losses help this, therefore synchronization and gear changing need less time. During downshift, synchronized gear is accelerated. Power losses still try to slow it down. Therefore, synchronization and changing need more time.

Table 1. Changing time vs. synchronized inertia, upshift

Changing	$0 \rightarrow 1$	$1 \rightarrow 2$	$2 \rightarrow 3$	$3 \rightarrow 4$	$4 \rightarrow 5$
Synchronized inertia [kgm^2]	0.061237	0.018798	0.009451	0.005736	0.005412
Changing time [s]	0.4498	0.2495	0.1998	0.1739	0.1709

Assuming the same synchronized inertia and initial conditions of gear changing, changing time decreases when synchronizing force maximum increases (*Fig. 9*).

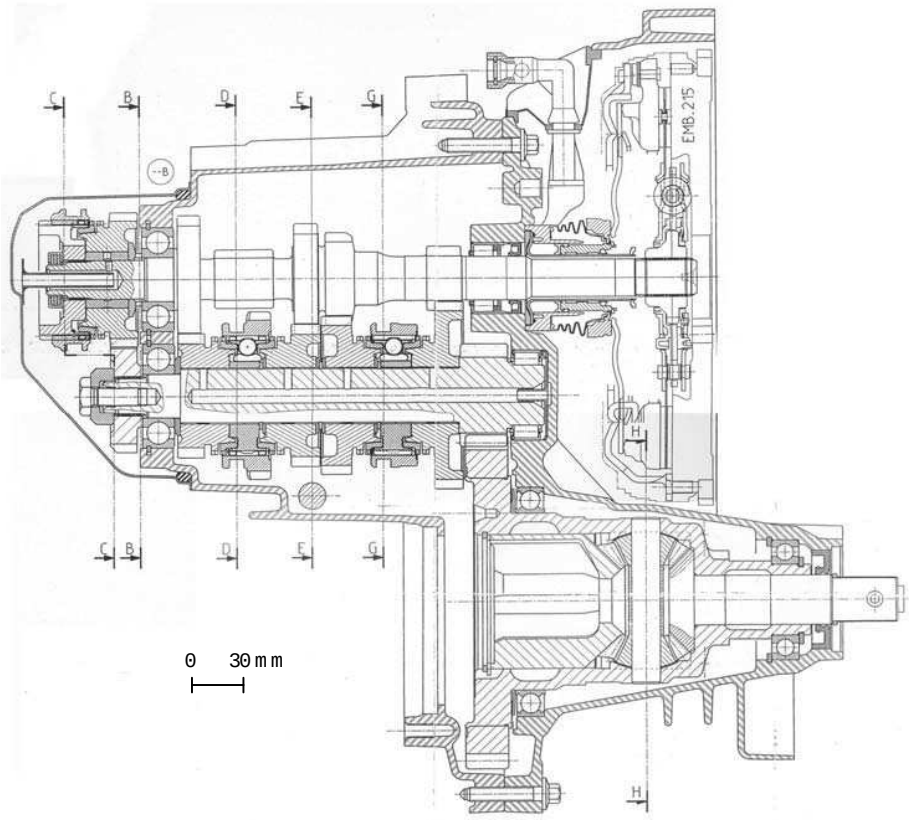

Fig. 7. General drawing of 5 speed JH gearbox

Table 2. Changing time vs. synchronized inertia, downshift

Changing	$5 \rightarrow 4$	$4 \rightarrow 3$	$3 \rightarrow 2$	$2 \rightarrow 1$
Synchronized inertia [kgm^2]	0.005736	0.009451	0.018798	0.061237
Changing time [s]	0.1804	0.2071	0.2581	0.4896

6. Study of the Second Bump Phenomena

6.1. Components of the Second Bump Force

As described in [8] and [10], synchro ring may stick on the gear cone at the end of the synchonization (3) phase. During the synchonization (3) phase, sleeve spline

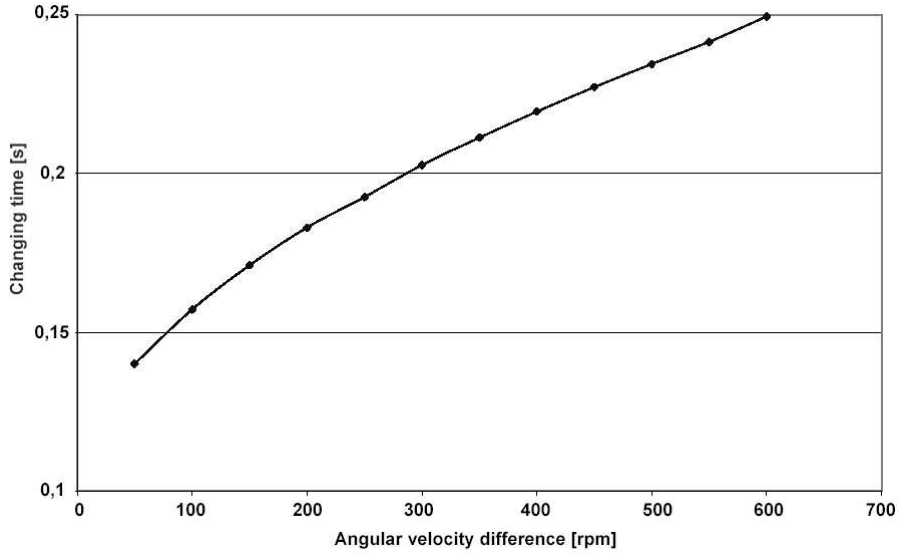

Fig. 8. Changing time variation vs. angular velocity difference, upshift 1 → 2

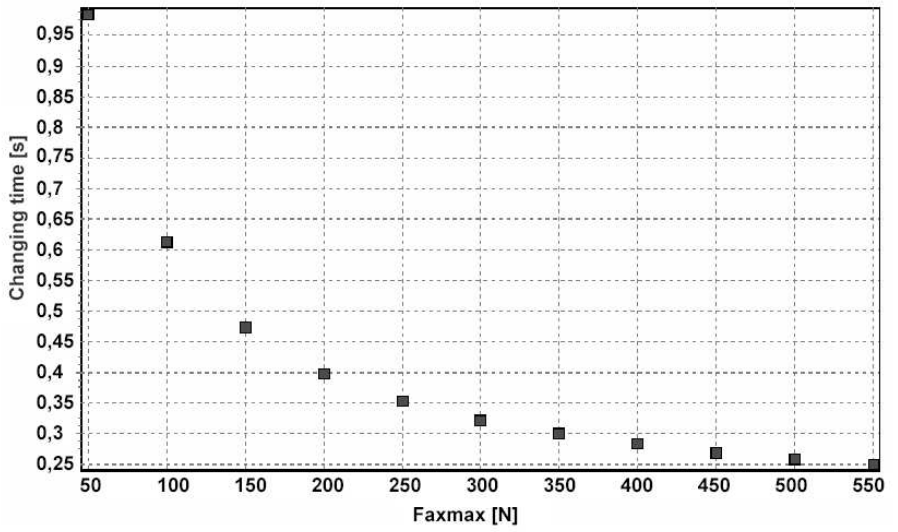

Fig. 9. Changing time vs. synchronizing force maximum, upshift 1 → 2

clutch teeth and synchro ring spline clutch teeth are in contact. Spline clutch teeth of the gear are not in contact with the sleeve spline teeth (*Fig. 10*). In the following figures, only the spline relative positions of the parts are represented. Splines are

represented by their sections with the common primitive cylinder, laid out in plane.

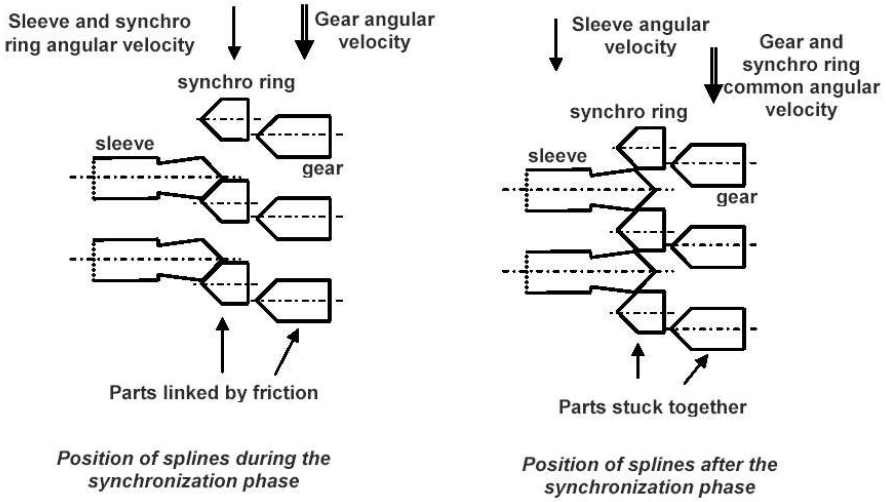

Fig. 10. Positions of the splines and angular velocities during and after the synchonization phase (schematic)

Having finished the synchonization (3) phase (*Fig. 10, Fig. 11*), synchro ring and gear (connected by the friction force on synchro cone) must be turned, allowing the sleeve spline to pass through the spline space. Thus, relative positions of the synchro ring spline teeth and the gear cone spline teeth remain fixed. In the next phases (turning the synchro ring (4), second free fly (5)) the sleeve moves forward axially and passes through the synchro ring.

Moving on the sleeve, sleeve splines meet gear spline chamfers. For allowing meshing, at first axial force is needed to separate synchro ring from the gear cone. In case of sticking influenced by random effects [10], [11], this axial force can be important. This force is produced at the end of the start of the second bump (6) phase. Having separated synchro ring and gear cone, the sleeve can turn the gear. The turning force depends on the relative angular position of gear splines and synchro ring splines.

The relatively high axial force needed for the separation of parts comes from the force equilibrium of stuck parts discussed in [10]. This force has an approximately deterministic part which is mainly determined by the following parameters:

- real synchro ring and gear conicity angles, giving the conicity angle error $\Delta\alpha$,
- synchro ring material elasticity,
- synchro ring structural elasticity,
- static friction coefficient between conical surfaces,

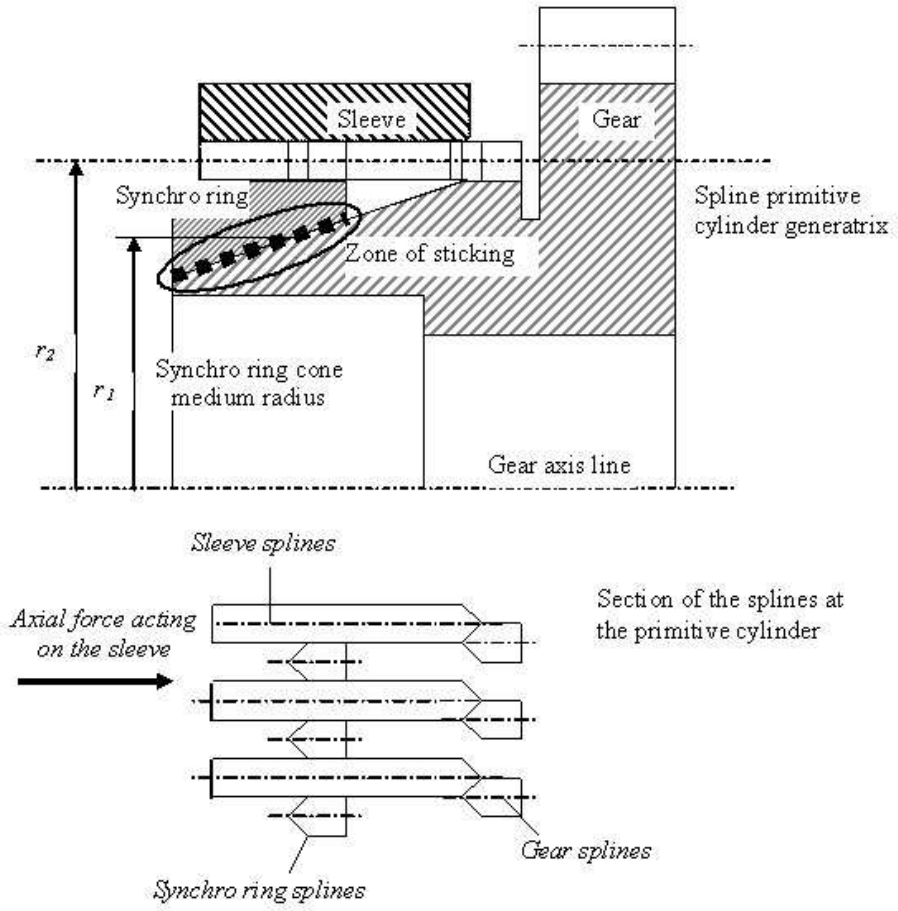

Fig. 11. Position of the parts at the moment of the second bump (schematic)

- friction coefficient on sleeve spline chamfers, gear spline chamfers, and synchro ring spline,
- sleeve and gear spline chamfer angles.

Random component of this force is due to the remaining axial force acting on the synchro ring. This latter is determined by friction forces acting on sleeve and hub spline mesh and centring mechanisms [8].

The turning force depends mainly on the relative position of gear and hub splines. This position is obtained at the end of the synchonization (3) phase, hence it is a random variable.

It is considered that the phenomenon mentioned generally as second bump is the combination of these two appearing high force values: the separating force and

the turning force. In measurements, it is practically impossible to distinguish them, because each appears for very short time, in successive working phases.

Separating and turning force components are further influenced by manufacturing error dispersion. Manufacturing of the gear cone and of the synchro ring imposes that tolerances are introduced on conicity angle of both parts. Separating force is considerably influenced by the conicity angle error $\Delta\alpha$ between the synchro ring conicity and the gear cone conicity [10].

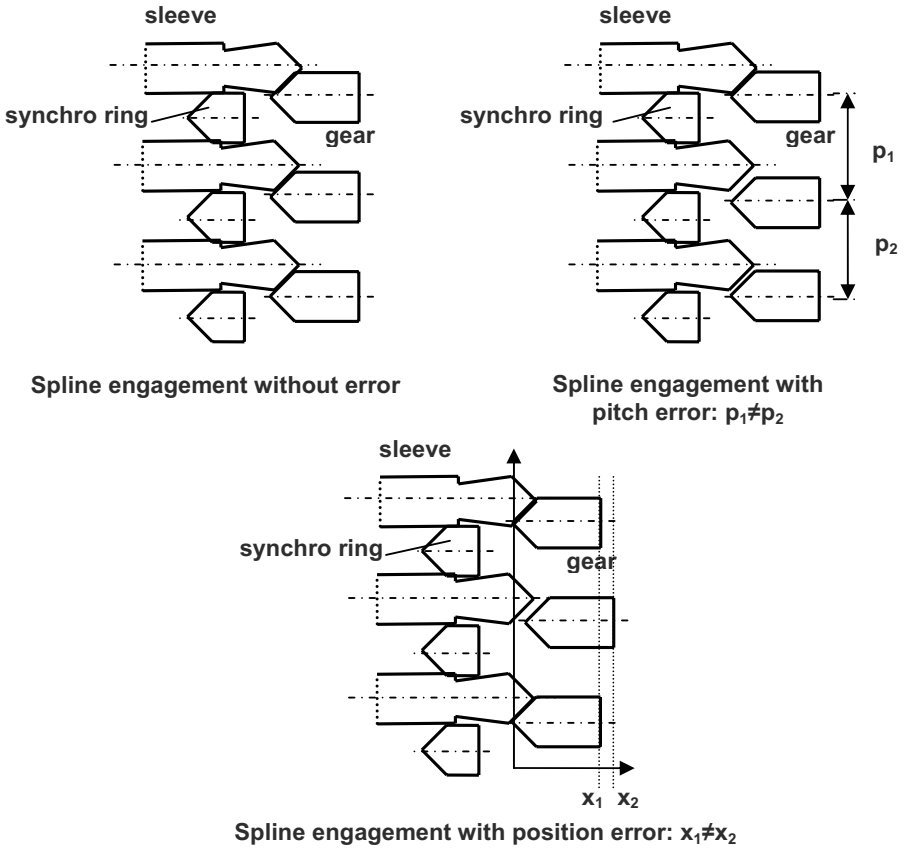

Fig. 12. Contact in case of splines with manufacturing errors

Other typical errors on splines are pitch error and position error. Such errors are present on splines of the gear, the synchro ring and the sleeve. When splines of two parts meet each other different types of contact can be realized, depending on the type of the manufacturing error. If there is no manufacturing error, contact is realized in the same time on all spline pairs (*Fig. 12*). If there is only position error, contacts are not realized in all spline pairs in the same time. Teeth slightly in front of the mean spline position enter in contact earlier, have more load, and suffer

heavier wear. Teeth slightly behind the mean position are charged during less time.

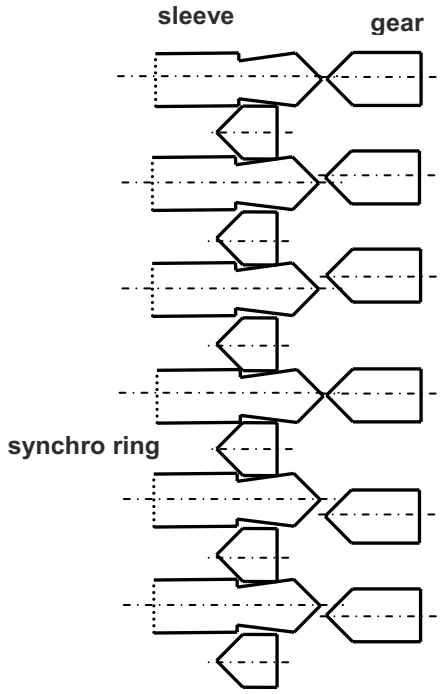

Fig. 13. Types of spline contact in case of pitch error

If there is only pitch error, the following problem can appear in case of relative spline position corresponding to the spline middle line. In the previous cases, contact sides on spline chamfers were always the same for all spline. In this case, some spline pairs have contact in the chamfer edge, others on the front side chamfer, another pairs on the rear side chamfer (*Fig. 13*). Continuation of the changing depends on the ratio of these contacts within the spline pairs. Wear and elasticity of the spline chamfer geometry have also influence on the continuation of the changing. Good choice of spline chamfer fillet radius r_f (*Fig. 14*), taking into account spline tolerances, can minimize problems due to contact differences and prevent not planned wear.

In this paper, spline teeth are considered errorless and identical on the part on which they are manufactured.

During synchonization, as it was presented earlier, the only link between the synchro ring and the gear cone is friction. Hence, at the end of the synchonization, relative position of sleeve and gear spline can be considered as random variable. In case of no systematic influence, the probability distribution of relative positions of gear and sleeve splines can be assumed as a uniform distribution.

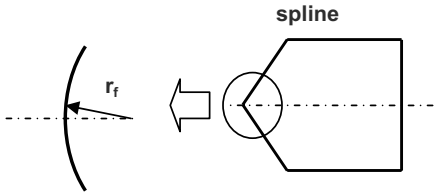

Fig. 14. Chamfer fillet

6.2. Determination of the Turning Axial Force

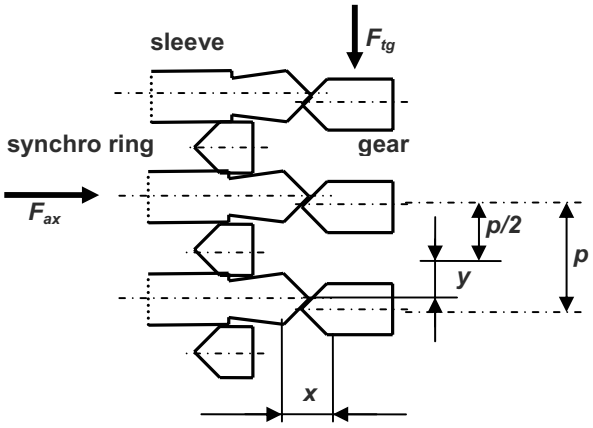

Fig. 15. Position of the splines at the start of turning the gear; x – axial displacement during turning, y – tangential displacement during turning

Let us consider two neighbouring gear and sleeve splines respectively (*Fig. 15*). In normal case, sleeve and gear angular velocities are equal, and sleeve moves in axial direction, towards the gear. Turning of the gear process is introduced by an impact on splines, and angular acceleration is imposed on the gear by spline contact, while sleeve continues to move. At the end of turning process, spline peak of sleeve is in the middle line of gear spline space (*Fig. 15*). Gear rotation is initiated by tangential force F_{tg} introduced by force F_{ax} , applied on sleeve.

For describing initial relative position of splines, variable y is introduced. It gives the distance of the sleeve spline peak from the middle line of the gear spline space, with pitch p. Value of y is measured in arc length on the pitch circle, and is a random variable.

To obtain engagement of gear and sleeve splines, rotation of the gear with arc length y must be realized. Depending on random relative position of splines

$-\frac{p}{2} \leq y \leq \frac{p}{2}$. In case of immediate engagement, $y = 0$. In case of maximal rotation, $y = \pm\frac{p}{2}$, and rotation of gear with angle $\pm\phi_R$ is needed. If $-\frac{p}{2} \leq y \leq 0$, then $\phi_R \leq 0$. If $0 < y \leq \frac{p}{2}$ then $\phi_R > 0$.

Let us define a non dimensional random variable ξ characterizing the relative position between the splines:

$$\xi = \frac{y}{p}. \tag{1}$$

Considering the geometry of the parts, two particular positions can be noted:

$$\text{If } y = 0 \qquad \xi = \frac{0}{p} = 0. \tag{2}$$

$$\text{If } y = \pm\frac{p}{2} \qquad \xi = \frac{\pm\frac{p}{2}}{p} = \pm\frac{1}{2}. \tag{3}$$

Hence $\xi = 0$ corresponds to mesh without impact. If $-\frac{1}{2} \leq \xi < 0$ then $\phi_R < 0$ and the gear must turn against the direction of its angular velocity (*Fig.16a*). If $0 < \xi \leq \frac{1}{2}$ then $\phi_R > 0$ and the gear must turn with the direction of its angular velocity (*Fig. 16b*).

In this, turning of the gear (7) phase, the sleeve moves forward with given axial velocity, imposed either by the driver or, in case of automatic command, an actuator. Displacement x of the sleeve during turning (*Fig. 15*), assuming time $t = 0$ and $x(0) = 0$ for the beginning of turning:

$$x = \int_0^t v_{ax}(t)\,\mathrm{d}t \tag{4}$$

with $t-$ time of turning the gear.

Relationship between axial and tangential displacement is the following:

$$x = \frac{y}{\operatorname{tg}\beta}, \tag{5}$$

where β – spline chamfer angle (*Fig. 17*).

A restriction coming from the previous equation is:

$$\operatorname{tg}\beta \neq 0. \tag{6}$$

Here $0 < \beta < 90^\circ$. Usual values are $\beta = 45..60^\circ$.

For further calculations the following assumptions are made:

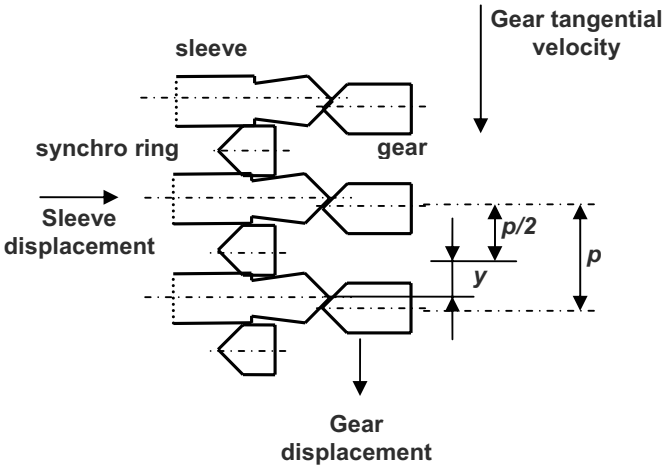

a) $\xi>0$

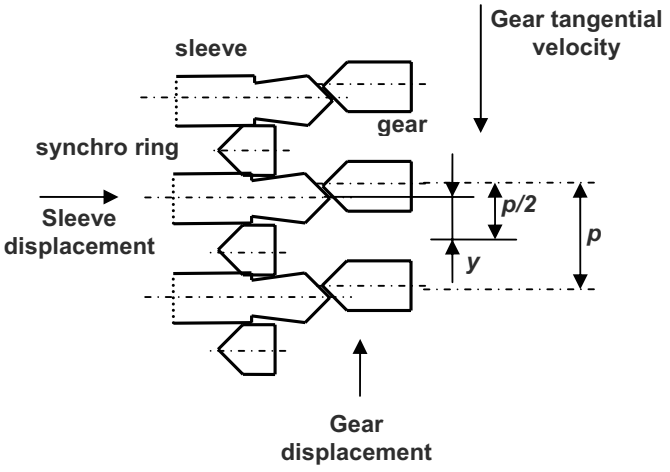

b) $\xi<0$

Fig. 16.

- the impact at entering into contact of gear and sleeve splines is neglected,
- during turning, gear rotation angular acceleration ε_R is constant,
- sleeve and gear splines are ideally rigid.

From measurement results (ex. *Fig. 2*) it can be concluded, that sleeve moves forward with almost constant axial velocity. Thus, accepting $v_{ax} = \text{const.}$, one can

write, from *Eq.* (4):

$$x = \int_0^t v_{ax}\,\mathrm{d}t = v_{ax} \cdot t. \tag{7}$$

Hence, the turning duration t:

$$t = \frac{x}{v_{ax}} \tag{8}$$

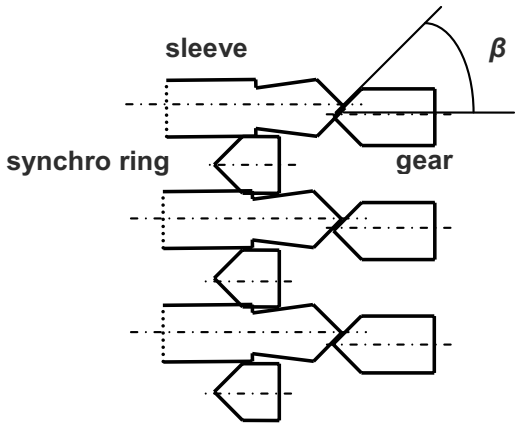

Fig. 17. Definition of the spline chamfer angle

Let us consider the turning angle of the gear from the tangential displacement:

$$\varphi_R = \frac{y}{r_2}, \tag{9}$$

where r_2 – spline primitive radius.

Let us express the turning angle from the angular acceleration:

$$\varphi_R = \frac{\varepsilon_R}{2} t^2. \tag{10}$$

Replacing *Eq.* (9) in *Eq.* (10):

$$\frac{y}{r_2} = \frac{\varepsilon_R}{2}\left(\frac{x}{v_{ax}}\right)^2 = \frac{\varepsilon_R}{2} \cdot \frac{y^2}{\mathrm{tg}^2\beta} \cdot \frac{1}{v_{ax}^2}. \tag{11}$$

Here, r_2 is different from zero. The axial velocity v_{ax} is non zero and is given as an input parameter.

After simplifying and transforming the *Eq.* (11), the following expression is obtained for angular acceleration:

$$\varepsilon_R = \frac{2 \cdot v_{ax}^2 \cdot \mathrm{tg}^2\beta}{y \cdot r_2}, \tag{12}$$

where $y \neq 0$. This restriction gives the case when theoretically no turning is possible, because sleeve spline chamfer edges meet gear spline chamfer edges. If no turning is possible, no angular acceleration will be present.

Expressing y from *Eq.* (1), and replacing y in *Eq.*(12):

$$\varepsilon_R(\xi) = \frac{2 \cdot v_{ax}^2 \cdot \mathrm{tg}^2\beta}{r_2} \cdot \frac{1}{\xi \cdot p}. \tag{13}$$

Here p is non zero. The following restriction must also be made:

$$\xi \neq 0. \tag{14}$$

If $\xi = 0$ then the sleeve is in the ideal meshing position. Meshing of the gear does not need turning, thus the angular acceleration will not exist.

Eq. (13) gives the angular acceleration needed for turning the gear, when power losses are not considered.

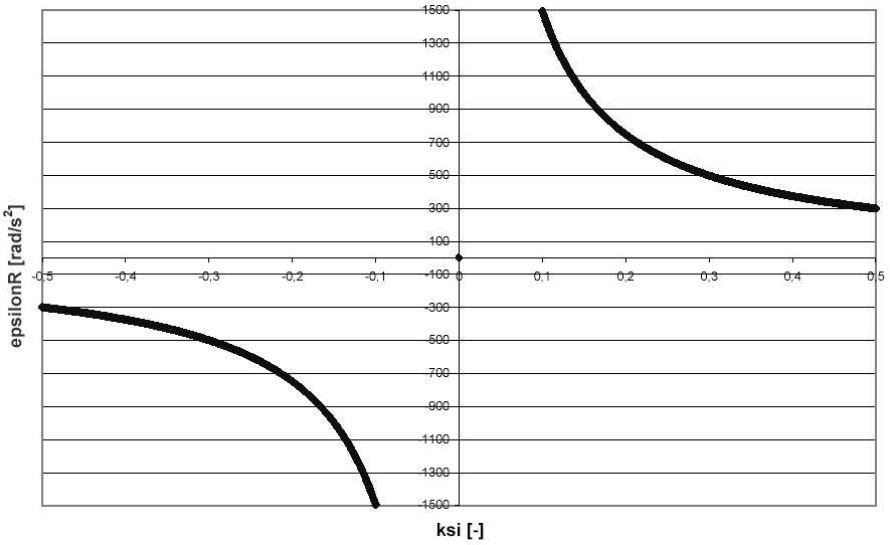

Fig. 18. Angular acceleration variation vs. ξ variation, no power losses considered, constant axial velocity

Fig. 18 represents the curve upon *Eq.* (16). The curve is symmetric to the $\xi = 0$ line. Near $\xi = 0$ the curve tends to the infinity. In the figure an upper limit of 1500 rad/s^2 and a lower limit of -1500 rad/s^2 are imposed, and angular acceleration values outside this interval are not shown. The equation completed with a value at the pole is:

$$\varepsilon_R(\xi) = \begin{cases} \dfrac{2 \cdot v_{ax}^2 \cdot \mathrm{tg}^2\beta}{r_2} \cdot \dfrac{1}{\xi \cdot p} & \text{if} \quad \xi \neq 0 \\ 0 & \text{if} \quad \xi = 0. \end{cases} \tag{15}$$

Upon the geometry, the curve should be symmetric to the $\xi = 0$ point (*Fig. 18*). But it is observed that the curves are not symmetric. Into a gearbox, turning of bearings and shafts in seals give power losses. Churning of gears in the oil also gives power losses. Together, these losses try to decrease angular velocity of turning parts. This effect can be useful during synchonization (3), turning the ring (4) or turning the gear (7) phases. Generally, if a part must be turned against the sense of revolution, power losses help turning, and for a given angular acceleration the needed external force is less than the theoretical one. If a part must be turned in the sense of revolution, power losses impeach turning and the needed external force for a given angular acceleration is more than the theoretical one.

In the studied case, when $\xi < 0$ power losses help turning, consequently external turning force can be smaller. When $\xi > 0$ power losses impeach turning, consequently external turning force should be higher. Power loss effects are clearly seen in *Fig. 19*.

Force needed for the turning can be computed from the tangential equilibrium of torques acting on the synchronized gear. Interacting torques are the power loss torques and torque from the tangential force issue from axial changing force. The equation for tangential equilibrium:

$$\theta_R \cdot |\varepsilon_R(\xi)| = \pm M_{\text{losses}}(\omega_R(t)) + M_{\text{tg}} \tag{16}$$

$$\theta_R \cdot |\varepsilon_R(\xi)| = \pm M_{\text{losses}}(\omega_R(t)) + F_{\text{tg}} \cdot r_2 \tag{17}$$

where ω_R – angular velocity of the synchronized gear,
θ_R – synchronized inertia reduced to the gear,
M_{losses} – torque of the power losses,
F_{tg} – tangential force,
f_3 – friction coefficient on gear spline chamfer.

For the loss torque, positive sign is used when $\xi > 0$ and negative sign is used when $\xi < 0$.

The well-known relationship between the axial and tangential forces [15]:

$$F_{ax} = F_{\text{tg}} \cdot \frac{f_3 + \mathrm{tg}\,\beta}{1 - f_3 \cdot \mathrm{tg}\,\beta} \tag{18}$$

From *Eqs.* (17) and (18), the general equation for the turning force can be obtained:

$$F_{ax} = \frac{\theta_R \cdot |\varepsilon_R(\xi)| \mp M_{\text{losses}}(\omega_R(t))}{r_2} \cdot \frac{f_3 + \mathrm{tg}\,\beta}{1 - f_3 \cdot \mathrm{tg}\,\beta} \tag{19}$$

This force depends on the initial relative position of gear splines and sleeve splines.

Fig. 19 shows simulated second bump peak force variation depending on ξ variation, upon equation (19). $\xi = +1/2$ and $\xi = -1/2$ cases are not represented, while $\xi = 0$ is shown. Two gear changing cases are represented: P1 $\rightarrow$ P2 means upshift, P2 $\rightarrow$ P1 means downshift. The second bump peak force is linked to the tangential turning force upon *Eq.* (18). Note that the highest force values are obtained near $\xi = 0$. Remember that at relative position $\xi = 0$ the turning force is zero. The figure illustrates the influence of the angular acceleration on the axial force.

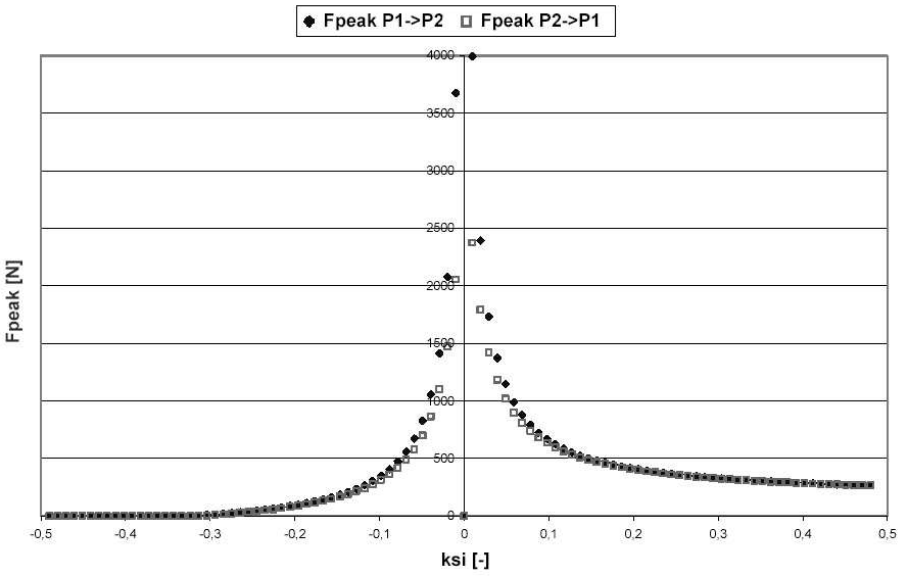

Fig. 19. Second bump peak force vs. relative spline position

6.3. Second Bump: Measurements and Simulations

For evaluation of calculated second bump force component for turning the gear, based on simplified model presented in 6.2., F_{ax} forces were calculated, with *Eq.* (19). Calculated force values were compared with second bump peak force values obtained by test rig measurements.

Synchronizer measurements were realized on a test rig as described in [8] and [10]. One synchronizer was studied. Changing was possible among three positions noted 'P1', 'neutral' and 'P2' respectively. Gear cones and synchro rings in positions P1 and P2 are different because of manufacturing tolerances and wear [10].

As expected, measured second bump force data issue from force measure-

ments have shown high dispersion. Measured peak values were sampled from a long test procedure. A data set of 37 elements was applied. Relative frequency diagram of a characteristic measured data set is represented on *Fig. 20*.

For F_{ax} second bump peak force value calculations by *Eq.* (19), mechanical and tribological parameters of test rig were applied, with constant sleeve displacement speed v_{ax}. For obtaining random relative position, ξ values were generated by random sampling, assuming uniform distribution function. Relative frequency diagram of calculated force values are represented in *Fig. 20*, for case of changing from position 2 to position 1 (P2 $\rightarrow$ P1). In *Fig. 20*, simulated and measured second bump force sets are shown as well.

One can state a relative good agreement between measured and simulated relative frequency diagrams, considering the relatively small number of sampling elements.

The only bigger difference can be seen in the class of 500 N force peaks. It means that in measurement, relative frequency of higher second bump forces is bigger as in calculation. Some reasons for this difference can be originated in some effects, not taken into consideration in calculation model.

As it was pointed out in 6.1, one component of second bump force is the axial force needed to release sticking of synchronizer cones, influenced by random effects as effective cone angle differences, remaining axial force on synchro ring (force applied to the synchro ring through the centring mechanisms persists during all the gear changing process [8]) etc. In calculations, synchro ring cone and gear cone are supposed to be ideal cones and axisymmetric on the same axis. However, in reality, they are not ideal cones, they can have non-parallel axis, and meet in such positions. Similarly, effect of randomly variable remaining axial push force on synchro ring is not taken into consideration. Both may increase the second bump force.

Further on, as measurements show, there is sometimes, in random manner, gear angular velocity desynchonization during turning the synchro ring (4) and second free fly (5) phases, giving increased additional effects. This is not included in the simulation, and may also increase the second bump force.

Second bump force peak can be influenced further by vibrations, introduced by mechanical parts of drive system, as ex. by gears or the changing process itself. These phenomena are not considered in the simulation and also can increase second bump force peak.

From a practical point of view, the forces represented in *Fig. 20* are applied on the sleeve, and exist in a short time period. The car driver applies changing force on the gear lever. Gear lever and the sleeve are linked with the gear changing mechanism. Inertia, elasticity and damping of the gear changing mechanism can modify the changing force variations present on the sleeve. Thus, the driver does not always feel such intense second bump force peaks.

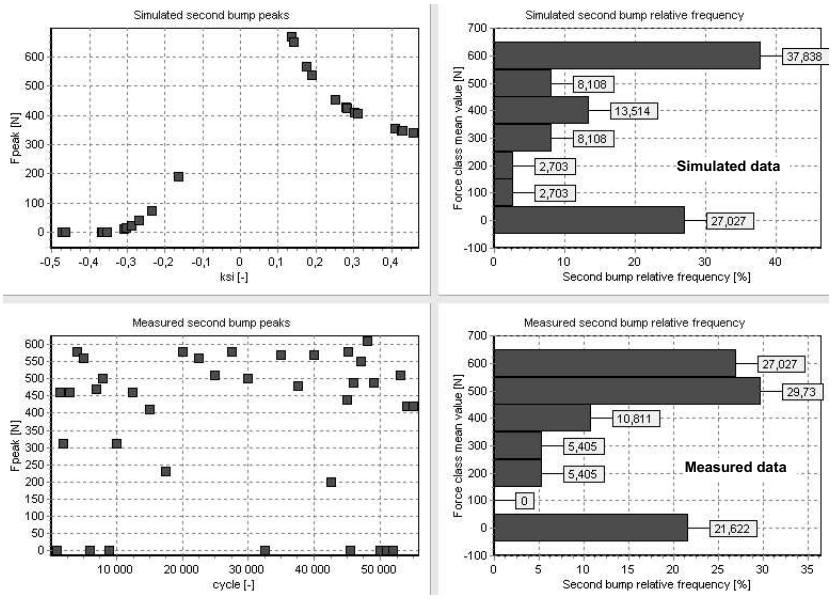

Fig. 20. Second bump peak values and relative frequency, changing P2 → P1

7. Conclusion

The work reported here permits to describe in detail the working phases of a synchronizer during gear changing process. Main mechanical parameters are taken into account to simulate the synchronizer behaviour. Numerical simulation software was designed to enable in a consistent way the study of parameter influence.

The results coming from numerical simulation allow to study effects of the most important parameters on gear changing process, giving an adequate tool for optimizing synchronizers in the design phase. Further on, detailed study of the so called second bump effect was presented, and its components: the force component to release sticking and the turning force were discussed. Numerical method was developed for the calculation of turning force. Taking into account the random nature of this second bump force component, comparative study was carried out between measured and calculated force values. Based on relative frequency diagrams, relatively good agreement was found. One should note that because of the immediate succession of the force components of second bump, and of the short time duration of the whole process, it is difficult to separate them by experimental tests. However, estimation of peak force values, based on model presented can be useful for designers, especially by development of robotized changing mechanisms.

Further research is needed for taking into account vibration effects in simulation models in one hand, and more detailed experimental study of this transient effect is to be realized on the other hand.

References

[1] ABDEL–HALIM, N. A. – BARTON, D. C. – CROLLA, D. A. – SELIM, A. M., Performance of Multicone Synchronizers for Manual Transmissions, *Proceedings of the Institution of Mechanical Engineers*, Part D, **214** (1997), pp. 55–65.

[2] D'ORAZIO, A. – CAUDANO, M. – UBERTI, M. – URBINATI, M., Multicone Synchronizer Dynamic Modelling and Experimental Bench Test Rig to Improve Manual Transmission Shiftability, *Proceedings of the JSME International Conference on Motion and Power Transmissions*, Fukuoka, Japan, nov. 15–17, 2001, pp. 649–656.

[3] HÖHN, B. R. – PINNEKAMP, B., Hochschaltkratzen bei kalten Pkw-Schaltgetrieben, VDI Berichte, 1995, Nr. 1175, pp. 435–451.

[4] HOSHINO, H., Simulation on Synchronisation Mechanism of Transmission Gearbox, *International ADAMS User Conference*, (1998), 7 p.

[5] KIM, J. – SUNG, D. – SEOK, C. – KIM, H. – SONG, H. – LIM, C. – KIM, J., Development of Shift Feeling Simulator for a Manual Transmission, SAE paper no. 2002-01-2202, 2002.

[6] KOGA, H. – ANZAI, K., Development of Manual Transmission 3-Cone Synchronizer, *JSAE Review*, **9** (4) (1988), pp. 102–104.

[7] LANZERATH, G. – PATZER, H., Synchronizer Blocker Ring with Organic Lining, SAE paper no. 860384, 1986, 11 p.

[8] LECHNER, G. – NAUNHEIMER, H., *Fahrzeuggetriebe*, Springer Verlag, 1994.

[9] LOVAS, L. – PLAY, D. – MÁRIALIGETI, J. – RIGAL, J.-F., Modelling Dynamical Processes in the Synchronization Process of Manual Gearboxes, (in Hungarian). *Gép*, Vol. LIV, 2003/10-11, pp. 103–109, ISSN 0016-85722002.

[10] LOVAS, L., *Etude des relations entre le fonctionnement et la fabrication des synchronisateurs des boîtes de vitesses manuelles.* PhD thesis, INSA-Lyon, 2004, 277 p.

[11] LOVAS, L. – PLAY, D. – MÁRIALIGETI, J. – RIGAL, J.-F., Internal Excitation and Effects in Gear Changing Process of Manual Automotive Gearboxes, In: PENNINGER, A., KULLMANN, L., VÖRÖS, G. eds., *'Gépészet 2004' Proceedings of the Fourth Conference on Mechanical Engineering*, Budapest University of Technology and Economics, 27–28 May 2004, Vol. II, pp. 573–577, ISBN 963 241 748 0.

[12] MCCORD, L., GYLON Friction Material for Transmission Synchronizers, *SAE paper* no. 860382, 1986, 8 p.

[13] MURATA, S. – MORI, Y. – DOI, T. – TAKADA, T. – NOGICHI, Y., Synchronizer and Shift System Optimization for Improved Manual Transmission Shiftability, *SAE paper* no. 891998, 1989, 12 p.

[14] OHTOMO, M., Synchronizer Rings Made of Resin and Iron Alloy for Pin-Ype Blocking Synchronizers Used in Heavy Vehicles, *JSAE Review*, **10** (4) (1989), pp. 71–74.

[15] SOCIN, R. – WALTERS, L. K., Manual Transmission Synchronizers, *SAE paper* no. 68008, 1968, 33 p.

[16] SYKES, L. M., The Jaguar XJ220 Triple-cone Synchronizer – A Case Study, *SAE Paper* No. 940737, 1994, 11 p.